

the first spin-allowed transitions of the trigonal and tetragonal complexes of the type $\text{Cr}^{\text{III}}(\text{N})_6$ in support of the theoretical approaches for the energy ordering and the rotational strengths. It is first demonstrated that room-temperature solution CD measurements can reveal the Kramers doublets of the ${}^2\text{E}_g$ state with a small spacing of less than 100 cm^{-1} . Within our present experimental and theoretical frameworks, the room-temperature

solution CD peaks observed near 15000 cm^{-1} are most likely attributed to the electronic origins of the spin-forbidden d-d transitions.

Acknowledgment. We thank Professor Yoichi Shimura of Osaka University for making the circular dichroism spectra available for the present work.

Contribution from the Christopher Ingold Laboratories, University College London, London WC1H 0AJ, U.K.

Resonance Raman Spectroscopy of the Manganate(VI) Ion: Band Excitation Profiles and Excited-State Geometry

ROBIN J. H. CLARK,* TREVOR J. DINES, and J. MARK DOHERTY

Received October 26, 1984

The resonance Raman spectrum of the manganate(VI) ion $[\text{MnO}_4]^{2-}$, isomorphously doped into $\text{K}_2[\text{CrO}_4]$, has been studied over the range 406.7–676.4 nm. Detailed excitation profiles have been measured for the $\nu_1(\text{a}_1)$ and $2\nu_1$ bands throughout the region of the charge-transfer band of lowest energy. Theoretical analysis of these excitation profiles demonstrates that, on excitation from the ground (${}^2\text{E}$) to resonant excited (${}^2\text{T}_2$) states, the Mn–O bond length increases by 0.035 \AA .

Introduction

In a number of recent papers^{1–5} we have reported the results of detailed resonance Raman studies of some transition-metal tetraoxo and tetrathio anions. The molecules studied were all d^0 complexes, and in each case excitation was resonant with the lowest energy electric dipole allowed charge-transfer transition, ${}^1\text{T}_2 \leftarrow {}^1\text{A}_1$. From a theoretical model described by Clark and Stewart¹ the geometric changes attendant upon excitation to the ${}^1\text{T}_2$ state were calculated from computer simulations of the resonance Raman excitation profiles of the bands attributed to the $\nu_1(\text{a}_1)$ fundamental and its overtones.

Having established the value of resonance Raman spectroscopy as a probe of the electronic structure of such molecules,⁶ it seemed appropriate to extend these studies to d^1 tetraoxo anions, of which the manganate(VI) ion, $[\text{MnO}_4]^{2-}$, may be regarded as the archetypal example. The molecular orbital scheme for $[\text{MnO}_4]^{2-}$ has been shown to be essentially the same as for $[\text{MnO}_4]^-$,^{7,8} and the extra electron is contained within the lowest energy antibonding orbital, which has e symmetry, giving rise to a ${}^2\text{E}$ ground term (cf. ${}^1\text{A}_1$ for $[\text{MnO}_4]^-$). As for $[\text{MnO}_4]^-$, the charge-transfer band of lowest energy results from the promotion of an electron from the t_1 nonbonding orbitals (localized on the oxygen atoms) to the e antibonding orbitals. The excited configuration $(t_1)^5(e)^2$ gives rise to two ${}^2\text{T}_1$, two ${}^2\text{T}_2$, and one ${}^4\text{T}_2$ terms (cf. ${}^1\text{T}_1$, ${}^1\text{T}_2$, ${}^3\text{T}_1$, and ${}^3\text{T}_2$ for $[\text{MnO}_4]^-$). Thus, there are four fully allowed transitions for $[\text{MnO}_4]^{2-}$, producing four strong absorption bands, in place of the single one for $[\text{MnO}_4]^-$. The absorption spectrum of $[\text{MnO}_4]^{2-}$ in the $15000\text{--}30000\text{-cm}^{-1}$ region has been assigned on the basis of calculations that put the energies of the excited terms in the order ${}^2\text{T}_2 < {}^2\text{T}_2 \sim {}^2\text{T}_1 < {}^2\text{T}_2$.^{8–10} There is also a weak

Table I. Band Wavenumbers of the $[\text{MnO}_4]^{2-}$ Ion Measured from Resonance Raman Spectra of $[\text{MnO}_4]^{2-}$ in $\text{K}_2[\text{CrO}_4]$ Recorded at ca. 15 K

assgnt	wavenumber/ cm^{-1}	assgnt	wavenumber/ cm^{-1}
$\nu_4(\text{t}_2)^a$	348 ± 1	$3\nu_1(\text{A}_1)$	2433.5 ± 0.5
$\nu_1(\text{a}_1)$	813.9 ± 0.5	$2\nu_1 + \nu_3(\text{T}_2)$	2452.6 ± 1.0
$\nu_3(\text{t}_2)$	832.3 ± 1.0	$4\nu_1(\text{A}_1)$	3235 ± 2
$2\nu_1(\text{A}_1)$	1625.5 ± 0.5	$3\nu_1 + \nu_3(\text{T}_2)$	3255 ± 2
$\nu_1 + \nu_3(\text{T}_2)$	1643.2 ± 0.5		

^a Overlapped by the $\nu_2(\text{e})$ band of the $[\text{CrO}_4]^{2-}$ ion.

band at around 12000 cm^{-1} assigned to the ${}^2\text{T}_2 \leftarrow {}^2\text{E}$ ligand field transition resulting from the promotion of the electron in the e antibonding orbital to the (next lowest energy) t_2 antibonding orbital. The energy of the ${}^4\text{T}_2$ state has not been determined, but it is probably less than those of the other four states.

There have been three previous resonance Raman studies of $[\text{MnO}_4]^{2-}$, all involving excitation within the region of the ${}^2\text{T}_2 \leftarrow {}^2\text{E}$ charge-transfer band of lowest energy. The results of these are summarized as follows: (1) a measurement of the excitation profiles of the ν_1 and $2\nu_1$ bands of $\text{K}_2[\text{MnO}_4]$ at room temperature;¹¹ (2) a study of the resonance Raman spectrum of $[\text{MnO}_4]^{2-}$ doped into CsI, recorded at 80 K, and a measurement of the excitation profile of the ν_1 band;¹² (3) wavenumber measurements of the resonance Raman bands of $\text{K}_2[\text{MnO}_4]$ and $\text{Ba}[\text{MnO}_4]$.¹³

The purpose of the present paper is to report, on the basis of dye laser excitation, the results of detailed measurements of the $\nu_1(\text{a}_1)$ and $2\nu_1$ Raman band excitation profiles. These measurements permit a more detailed analysis to be made of the charge-transfer band of lowest energy and permit an evaluation of the geometric change attendant upon excitation to the lowest ${}^2\text{T}_2$ state. Resonance Raman spectra were obtained from samples of $[\text{MnO}_4]^{2-}$ isomorphously doped into $\text{K}_2[\text{CrO}_4]$, for which extensive electronic absorption data have been reported by Day et al.¹⁴

Experimental Section

$\text{K}_2[\text{MnO}_4]$ was prepared by using the method of Nyholm and Woolliams.¹⁵ Crystals of $[\text{MnO}_4]^{2-}$ doped into $\text{K}_2[\text{CrO}_4]$ were grown by slow

- Clark, R. J. H.; Cobbold, D. G.; Stewart, B. *Chem. Phys. Lett.* **1980**, *69*, 488. Clark, R. J. H.; Stewart, B. *J. Am. Chem. Soc.* **1981**, *103*, 6593.
- Clark, R. J. H.; Dines, T. J.; Wolf, M. L. *J. Chem. Soc., Faraday Trans. 2* **1982**, *78*, 679.
- Clark, R. J. H.; Dines, T. J. *J. Chem. Soc., Faraday Trans. 2* **1982**, *78*, 723.
- Clark, R. J. H.; Dines, T. J. *Inorg. Chem.* **1982**, *21*, 3585.
- Clark, R. J. H.; Dines, T. J.; Proud, G. P. *J. Chem. Soc., Dalton Trans.* **1983**, 2019.
- Clark, R. J. H. *ACS Symp. Ser.* **1983**, No. 211, 509.
- Ziegler, T.; Rauk, A.; Baerends, E. *J. Chem. Phys.* **1976**, *16*, 209.
- Jasinski, J. P.; Holt, S. L. *J. Chem. Soc., Faraday Trans. 2* **1976**, *72*, 1304.
- DiSipio, L.; Oleari, L.; Day, P. *J. Chem. Soc., Faraday Trans. 2* **1972**, *68*, 776.
- Vanquickenborne, L. G.; Verdonck, E. *Inorg. Chem.* **1976**, *15*, 454.

- Chao, R. S.; Khanna, R. K.; Lippincott, E. R. *J. Raman Spectrosc.* **1975**, *3*, 121.
- Martin, T. P.; Onari, S. *Phys. Rev. B: Solid State* **1977**, *15*, 1093.
- Jubert, A. H.; Varetto, E. L. *J. Mol. Struct.* **1982**, *79*, 285.
- Day, P.; DiSipio, L.; Ingletto, G.; Oleari, L., *J. Chem. Soc., Dalton Trans.* **1973**, 2595.
- Nyholm, R. S.; Woolliams, P. R. *Inorg. Synth.* **1968**, *11*, 57.

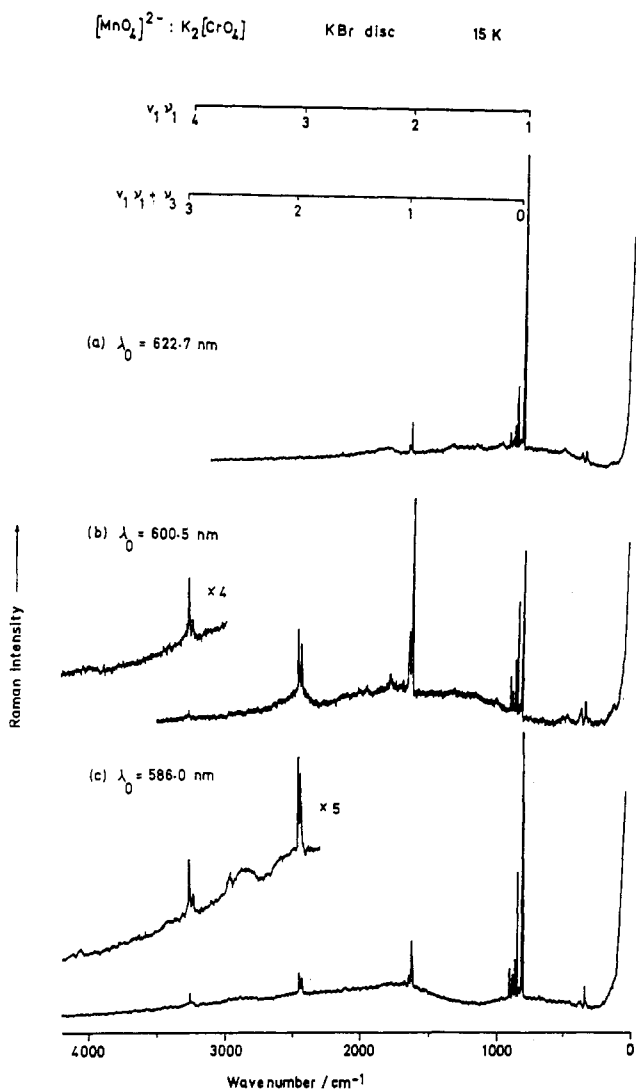


Figure 1. Resonance Raman spectra of $[\text{MnO}_4]^{2-}$ in the $\text{K}_2[\text{CrO}_4]$ host lattice, recorded at 15 K with 586.0-, 600.5-, and 622.7-nm excitation.

evaporation of aqueous 10 M KOH solutions of $\text{K}_2[\text{CrO}_4]$ containing a low concentration of $\text{K}_2[\text{MnO}_4]$. The concentration of $[\text{MnO}_4]^{2-}$ in the crystals was determined spectrophotometrically to be in the range 1–1.5%. Resonance Raman spectra were obtained from KBr disks held at either ca. 15 K (Air Products Displex cryostat) or ca. 80 K (liquid-nitrogen-cooled cell), the laser power at the sample not exceeding 100 mW.

Raman spectra were recorded on Spex 1401 and 14018 (Ramalog 6) spectrometers in conjunction with Coherent Radiation Model Innova-12 argon ion and CR3000K krypton ion lasers and a CR490 dye laser employing rhodamine 6G as the lasing medium. Detection of the scattered radiation was by standard photon-counting techniques using RCA C31034 photomultipliers. Wavenumber measurements were calibrated by reference to the emission spectrum of neon. Band intensities were determined as the products of peak heights and full width half-maxima (fwhm) and corrected for the spectral response of the appropriate instrument. Resonance Raman excitation profiles were constructed with the $\nu_1(a_1)$ band of $\text{K}_2[\text{CrO}_4]$ as an internal standard.

Electronic absorption spectra were recorded on a Cary 14 spectrometer from KBr disks at ca. 15 K using an Air Products Displex cryostat.

Results and Discussion

Resonance Raman Spectra. Resonance Raman spectra of $[\text{MnO}_4]^{2-}$ in the $\text{K}_2[\text{CrO}_4]$ host lattice, recorded at 15 K using 586.0-, 600.5-, and 622.7-nm excitation, are shown in Figure 1. Measurements of the band wavenumbers and their assignments are listed in Table I. The salient features of these spectra are summarized as follows:

(1) Two progressions, $\nu_1\nu_1$ extending to $\nu_1 = 4$ and $\nu_1\nu_1 + \nu_3$ to $\nu_1 = 3$, are noted. The intensities of the members of the latter progression increase with respect to those of the former with

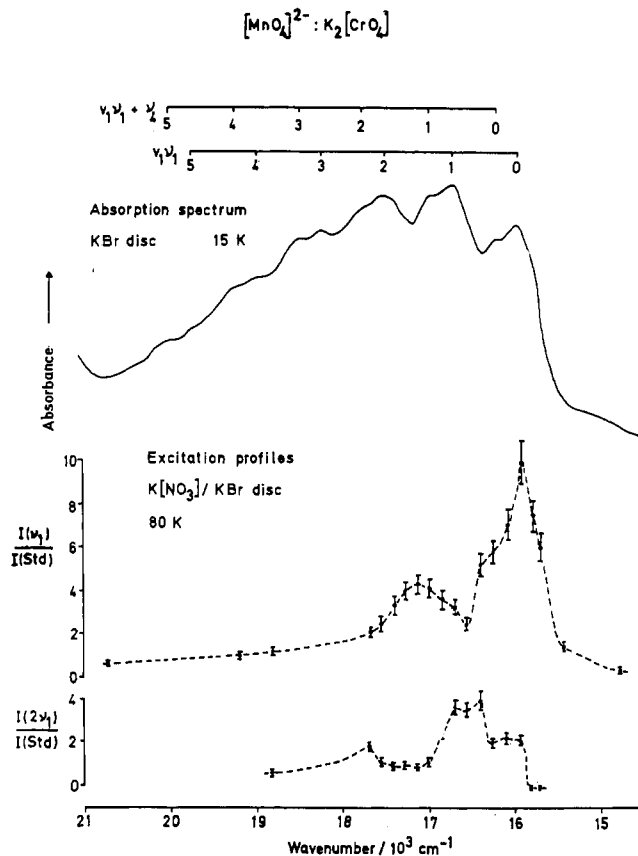


Figure 2. Electronic absorption spectrum of $[\text{MnO}_4]^{2-}$ as a KBr disk at ca. 15 K, together with the ν_1 and $2\nu_1$ band excitation profiles of $[\text{MnO}_4]^{2-}$ as a KNO_3/KBr disk at ca. 80 K.

increasing ν_1 . For example $I(\nu_3)/I(\nu_1) = 0.03$ and $I(3\nu_1 + \nu_3)/I(4\nu_1) = 3$ with 586.0-nm excitation.

(2) A weak band at 348 cm^{-1} is assigned to $\nu_4(t_2)$ although it is overlapped by the $\nu_2(e)$ band of the $[\text{CrO}_4]^{2-}$ ion. No progressions involving this fundamental were observed.

(3) A weak luminescence background containing several ill-defined peaks is seen. This is too high in energy to be assigned to emission from the 2T_2 ligand field state but could be from the 4T_2 state, whose energy has not yet been determined.

Standard analysis of the band wavenumbers of the observed progressions, within the usual approximations,¹⁶ provides the following ground-state vibrational constants: $\omega_1 = 817.7 \pm 0.5\text{ cm}^{-1}$, $x_{11} = -1.7 \pm 0.2\text{ cm}^{-1}$, and $x_{13} = -2.0 \pm 0.5\text{ cm}^{-1}$. Thus, in common with most tetrahedral species, ν_1 behaves very nearly as an harmonic oscillator in the ground state.

Notwithstanding the low site symmetry (C_s) of $[\text{MnO}_4]^{2-}$ in the $\text{K}_2[\text{CrO}_4]$ host lattice, there is no evidence of splitting of the triply degenerate fundamentals ν_3 and ν_4 , indicating that the perturbation is very small. The presence of these bands in the resonance Raman spectrum is due to Jahn–Teller effects in the 2T_2 excited state, involving these two normal coordinates. The observation of the progression $\nu_1\nu_1 + \nu_3$ is clear evidence for a strong Jahn–Teller distortion along the normal mode Q_3 in the excited state, especially in view of the above-mentioned intensity distribution for this progression.

Excitation Profiles and Absorption Spectrum. Raman spectra were recorded with excitation in the region 406.7–676.4 nm, and excitation profiles were constructed for ν_1 and $2\nu_1$ with the $\nu_1(a_1)$ band of the $[\text{CrO}_4]^{2-}$ ion as an internal intensity standard. Although the latter undergoes preresonance enhancement throughout the region of excitation, it was possible to make a correction for this effect from the data of Kiefer and Bernstein¹⁷ and Tsuboi and Hirakawa.¹⁸ The excitation profiles are shown in Figure 2

(16) Clark, R. J. H.; Stewart, B. *Struct. Bonding (Berlin)* 1979, 36, 1.

(17) Kiefer, W.; Bernstein, H. *J. Mol. Phys.* 1972, 23, 835.

together with the absorption spectrum recorded at 15 K. The latter displays progressions $\nu_1\nu_1$ (average spacing $750 \pm 10 \text{ cm}^{-1}$) and $\nu_1\nu_1 + \nu_4$ (average value for ν_4 is $250 \pm 10 \text{ cm}^{-1}$), and the wavenumber of the 0-0 transition is $16010 \pm 10 \text{ cm}^{-1}$. The presence of the $\nu_1\nu_1 + \nu_4$ progression is due to the Jahn-Teller activity of ν_4 in the excited state. The resonance Raman data indicate that the excited-state Jahn-Teller distortion is greater for the asymmetric stretching vibration ν_3 , a fact that cannot be deduced from the absorption spectrum because ν_3 is too close to ν_1 to be resolved. This is a good illustration of the superiority of resonance Raman spectroscopy as a probe of excited-state Jahn-Teller effects.

The excitation profiles of the ν_1 and $2\nu_1$ Raman bands display vibrational fine structure, but of markedly different appearance from that of the absorption band. This is due to interference effects between the contributions to the transition polarizability from the individual vibronic resonances, an effect that has been demonstrated for several other species, a particularly striking example being that of $[\text{MnO}_4]^-$.¹ From an established theoretical model for A-term resonance Raman scattering,^{1,16} it is possible to calculate the excitation profiles of bands attributed to totally symmetric modes and their overtones. Such calculations involve parameters relating to properties of the resonant excited state, and by determining a best fit calculation to the experimental data, it may be possible to quantify geometric changes attendant upon excitation to the resonant state.

Where only a single resonant state $|e\rangle$ contributes significantly, the transition polarizability for quanta of the totally symmetric mode of a tetrahedral MX_4 molecule is given by eq 1, where $|g\rangle$

$$[\alpha_{\rho\rho}]_{gn, g0} = \frac{1}{\hbar c} |[\mu_{\rho}]_{ge}|^2 \sum_v \frac{\langle n_g | v_e \rangle \langle v_e | 0_g \rangle}{\bar{\nu}_{ev, g0} - \bar{\nu}_0 + i\Gamma_{ev}} \quad (1)$$

is the ground electronic state, n and v are vibrational quantum numbers, and Γ_{ev} represents the homogeneous line width, which is inversely proportional to the lifetime of the ion in the v th level of the resonant excited state. In using this equation it is assumed that (1) the Born-Oppenheimer approximation is valid, (2) the dependence of the transition dipole moment on the normal coordinates may be neglected (Condon approximation), (3) all molecules are initially in the zeroth vibrational level (low-temperature limit), and (4) the nonresonant part of the polarizability may be neglected. Variation of the electronic transition wavenumbers $\bar{\nu}_{ev, g0}$ with molecular environment (i.e. inhomogeneous broadening) is accounted for by convolution of the transition polarizability with a line-shape function $\mathcal{L}(\bar{\nu})$:

$$[\alpha_{\rho\rho}]_{gn, g0} = \frac{1}{\hbar c} |[\mu_{\rho}]_{ge}|^2 \int_{-\infty}^{\infty} \left[\sum_v \frac{\langle n_g | v_e \rangle \langle v_e | 0_g \rangle}{\bar{\nu}_{ev, g0} - \bar{\nu}_0 + i\Gamma_{ev}} \right] \mathcal{L}(\bar{\nu}_{eg}) d\bar{\nu}_{eg} \quad (2)$$

In the present study the line-shape function has been assumed to be Lorentzian

$$\mathcal{L}(\bar{\nu}_{eg}) = \gamma [(\bar{\nu}_{eg} - \langle \bar{\nu}_{eg} \rangle)^2 + \gamma^2]^{-1} \quad (3)$$

where $\langle \bar{\nu}_{eg} \rangle$ is the average value of the electronic transition wavenumber and γ is the inhomogeneous line width. The integral in eq 2 has been evaluated by Siebrand and co-workers,^{19,20} and excitation profiles may be calculated from eq 4, where $\epsilon_v = \bar{\nu}_{ev, g0}$

$$I_{gn, g0} \left(\frac{\pi}{2} \right) = K (\bar{\nu}_0 - \nu_{gn, g0})^4 |[\mu_{\rho}]_{ge}|^4 \sum_v \sum_{v'} \langle n_g | v_e \rangle \langle v_e | 0_g \rangle \langle n_g | v_e' \rangle \langle v_e' | 0_g \rangle \left\{ \frac{[(\epsilon_v - \epsilon_{v'})^2 + 4\Gamma\Sigma][\epsilon_v\epsilon_{v'} + \Sigma^2] - 2(\epsilon_v - \epsilon_{v'})\gamma\Sigma}{[\epsilon_v^2 + \Sigma^2][\epsilon_{v'}^2 + \Sigma^2][(\epsilon_v - \epsilon_{v'})^2 + 4\Gamma^2]} \right\} \quad (4)$$

$-\bar{\nu}_0$ and $\Sigma = \Gamma + \gamma$. In this equation it has been assumed that the homogeneous line width is the same for all vibrational levels of the excited state. This is not a necessary assumption (nor strictly

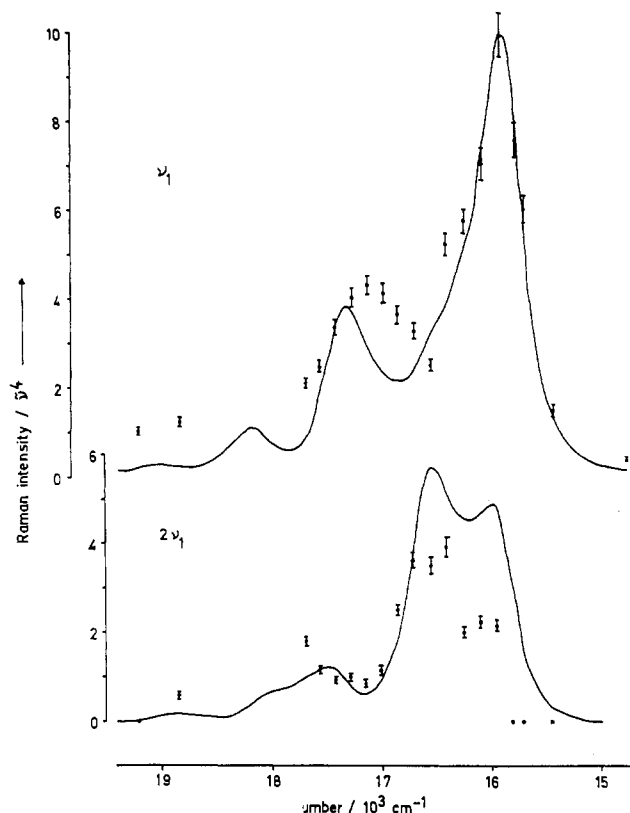


Figure 3. Experimental and calculated excitation profiles for the ν_1 and $2\nu_1$ bands of $[\text{MnO}_4]^{2-}$.

Table II. Parameters Used in the Calculation of the Excitation Profiles

$\bar{\nu}_0^g$	815 cm^{-1}	Δr	0.035 ± 0.001
$\bar{\nu}_1^e$	750 cm^{-1}	Γ	$250 \pm 10 \text{ cm}^{-1}$
$\bar{\nu}_{00}$	15900 cm^{-1}	γ	0 cm^{-1}
ΔQ	$0.28 \pm 0.01 \text{ \AA amu}^{1/2}$		

valid), but it considerably simplifies the calculations. It is not expected to cause any significant errors within the framework of the approximations made.

The vibrational overlap integrals $\langle n_g | v_e \rangle$ and $\langle v_e | 0_g \rangle$ are calculated from Manneback's recursion formulas.²¹ They are dependent on the ground- and excited-state wavenumbers for the ν_1 mode ($\bar{\nu}_1^g$ and $\bar{\nu}_1^e$) and the displacement ΔQ_1 of the excited-state potential energy minimum, with respect to that of the ground state, along the normal-coordinate Q_1 . The latter is related to the bond length extension, Δr , attendant upon excitation to the resonant state.

Using eq 4, we have calculated excitation profiles for the ν_1 and $2\nu_1$ bands, in the region of the ${}^2\text{T}_2 \leftarrow {}^2\text{E}$ charge-transfer band. The best fit obtained is shown in Figure 3, together with the experimental data, and the values of the parameters used in the calculations are listed in Table II. Although the calculated excitation profiles do not fit the experimental data very well, they do faithfully reproduce certain features, in particular the positions of the maxima and minima, the inflection in the ν_1 profile at ca. 16250 cm^{-1} , and the high intensity of $2\nu_1$ (relative to ν_1) in the 16500-cm^{-1} region.

The value of $\Delta r = 0.035 \text{ \AA}$ is smaller than that obtained from a Franck-Condon analysis of the absorption band, for which $\Delta r \approx 0.04 \text{ \AA}$ would be required to reproduce the intensity distribution in Figure 2. Day et al.¹⁴ compute a value of $\Delta^2 = 1.45 \pm 0.10$ for $[\text{MnO}_4]^{2-}$ in three alkali-metal sulfate host lattices, where $\Delta^2 = 8\pi^2 c \bar{\nu} \mu (\Delta r)^2 / \hbar$, $\bar{\nu}$ is the vibrational wavenumber, assumed to be the same for the ground and excited states, and μ is the reduced mass associated with the vibration.²² From this analysis it is

(18) Tsuboi, M.; Hirakawa, A. Y. *J. Mol. Spectrosc.* **1975**, *56*, 146.

(19) Penner, A. P.; Siebrand, W. *Chem. Phys. Lett.* **1976**, *39*, 11.

(20) Siebrand, W.; Zgierski, M. Z. *J. Phys. Chem.* **1982**, *86*, 4718.

(21) Manneback, C. *Physica* **1951**, *17*, 1001.

Table III. Bond Length Changes (Δr) in Tetrahedral Ions on Excitation

ion	resonant transition	$\Delta r/\text{\AA}$	ref
$[\text{MnO}_4]^-$	${}^1\text{T}_2 \leftarrow {}^1\text{A}_1$	0.046	1
$[\text{MnO}_4]^{2-}$	${}^2\text{T}_2 \leftarrow {}^2\text{E}$	0.035	this work
$[\text{MoS}_4]^{2-}$	${}^1\text{T}_2 \leftarrow {}^1\text{A}_1$	0.035	2
$[\text{WS}_4]^{2-}$	${}^1\text{T}_2 \leftarrow {}^1\text{A}_1$	0.029	5

calculated that $\Delta r = 0.044 \pm 0.002 \text{ \AA}$. Martin and Onari¹² fitted their resonance Raman data by a Franck-Condon analysis using a value of $\Delta^2 = 3.0$. This corresponds to a bond length change $\Delta r = 0.063 \text{ \AA}$, which is clearly too large. The higher Δr values obtained from the analysis of the absorption spectra are most probably due to the overlap of the main $\nu_1\nu_1$ progression by $\nu_1\nu_1 + \nu_3$. The latter is not resolved because of the close proximity of ν_1 to ν_3 but must nevertheless be present (vide supra). Its presence would increase the intensities of the 0_g-0_g peaks relative to that of the 0_g-0_g one, thus producing an erroneously high value for Δr .

The bond length changes in tetrahedral ions attendant upon excitation to the lowest (electric dipole allowed) charge-transfer state are given in Table III. The values listed are a factor of 2 smaller than those given in the original electronic²² and resonance Raman papers^{1,2,5} owing to the use in these papers of an incorrect

relation between Δr and ΔQ_1 . The bond length change calculated for $[\text{MnO}_4]^{2-}$ is $\sim 25\%$ lower than that for $[\text{MnO}_4]^-$. It is not clear why this should be since, in both cases, the excitation involves the same pair of orbitals. Moreover, Δr for $[\text{MnO}_4]^-$ is about 50% greater than that established crystallographically (0.03 \AA) to accompany one-electron reduction of $[\text{MnO}_4]^-$ to $[\text{MnO}_4]^{2-}$, each in their ground state.²³ In common with $[\text{MnO}_4]^-$ the excitation profiles are best reproduced by assuming that the broadening mechanism is exclusively homogeneous. Introduction of inhomogeneous broadening resulted in much higher value for $I(2\nu_1)/I(\nu_1)$ in the preresonance region than is observed experimentally. Introduction of inhomogeneous broadening resulted in much higher value for $I(2\nu_1)/I(\nu_1)$ in the preresonance region than is observed experimentally.

No resonance enhancement was observed for excitation within the contour of the next strong absorption band of the $[\text{MnO}_4]^{2-}$ ion, at around 24000 cm^{-1} . This absorption results from the superposition of the second lowest energy ${}^2\text{T}_2 \leftarrow {}^2\text{E}$ band and the lowest energy ${}^2\text{T}_1 \leftarrow {}^2\text{E}$ band. The lack of resonance enhancement in this region may be due to destructive interference between the contributions to the transition polarizability from the ${}^2\text{T}_2$ and ${}^2\text{T}_1$ and other nearby states.

Acknowledgment. The authors are indebted to the SERC and University of London (ULIRS) for financial assistance.

Registry No. $[\text{MnO}_4]^{2-}$, 14333-14-3; $\text{K}_2[\text{CrO}_4]$, 7789-00-6.

(22) Ballhausen, C. J. *Theor. Chim. Acta* 1963, 1, 285.

(23) Palenik, G. J. *Inorg. Chem.* 1967, 6, 503, 507.

Contribution from the Laboratoire de Chimie de Coordination du CNRS associé à l'Université P. Sabatier, 31400 Toulouse, France

Metal Complexes of Rubenic Acid. 3.¹ Large-Angle X-ray Scattering Studies of Amorphous Copper(II) and Nickel(II) Complexes

MOSTAFA ABBOUDI, ALAIN MOSSET, and JEAN GALY*

Received July 9, 1984

Two amorphous complexes of the dithiooxamide ligand (rubenic acid) have been prepared and studied: $\text{Cu}(\text{C}_2\text{S}_2\text{N}_2\text{H}_2)(\text{H}_2\text{O})$ and $\text{Ni}_4(\text{C}_2\text{S}_2\text{N}_2\text{H}_2)_2(\text{C}_2\text{S}_2\text{N}_2\text{H}_2)_3(\text{H}_2\text{O})_{0.25}$. Both compounds have essentially the same local structure. The proposed structural model can be described by the following features: (i) the ligand is in a trans conformation and planar; (ii) the coordination is ensured by the four donor atoms (S, N), and the Ni environment is square planar; (iii) the ribbons thus formed stack perpendicularly to the ligand plane with an interval equal to 3.6 \AA .

Introduction

The complexes of rubenic acid (dithiooxamide) have been used in analytical chemistry for a long time,^{2,3} but their magnetic,⁴ semiconducting,⁵ and catalytic⁶ properties have only recently been accounted for and have induced new searches on their structure. Very little is known about their geometry due to the extreme difficulty in growing single crystals; the metallic complexes of the nonsubstituted rubenic acid are insoluble in most common solvents. Consequently, they are always obtained in the amorphous state or as a very poorly crystalline powder. Numerous solution- and solid-state studies have been performed by using various

Table I. Chemical Analysis of the Copper and Nickel Complexes

M		C	H	N	S	M
Cu	% found	12.85	1.55	14.13	33.78	32.5
	% calcd ^a	12.02	2.01	14.02	32.10	31.8
Ni	% found	13.99	1.65	15.83	35.16	27.88
	% calcd ^a	14.16	1.66	16.51	37.80	27.68

^a Calculated with respect to the formulas $\text{Cu}(\text{C}_2\text{N}_2\text{S}_2\text{H}_2)(\text{H}_2\text{O})$ and $\text{Ni}_4(\text{C}_2\text{N}_2\text{S}_2\text{H}_2)_2(\text{C}_2\text{H}_2\text{S}_2\text{H}_2)_3$.

spectroscopic methods to settle the systematics of the coordination modes of the rubenic acid ligand.⁷⁻⁹ These studies proposed various structural hypotheses, but it has not been made possible to check them through an experimental single-crystal X-ray diffraction investigation.

(1) Parts 1 and 2: Mosset, A.; Abboudi, M.; Galy, J. Z. *Crystallogr.* 1983, 164, 171, 181.

(2) Ray, P.; Ray, R. M. *Q. J. Indian Chem. Soc.* 1926, 118, 26.

(3) Ray, P.; Xavier, J. J. *Indian Chem. Soc.* 1961, 38, 535.

(4) Kanekar, C. R.; Casey, A. T. *J. Inorg. Nucl. Chem.* 1969, 31, 3105.

(5) Kanda, S.; Suzuki, A.; Ohkawa, K. *Energy Charge Transfer Org. Semicond., Proc. U.S.-Jpn. Semin.* 1973, 85.

(6) Batur, D. G.; Reibel, I. M.; Sandu, A. F. *Koord. Khim.* 1981, 7, 149.

(7) Peyronel, G.; Pellacani, G. C.; Pignedoli, A. *Inorg. Chim. Acta* 1971, 5, 627.

(8) Pellacani, G. C.; Peyronel, G. *Inorg. Chim. Acta* 1974, 9, 189.

(9) Hofmans, H.; Dessey, H. O.; Herman, M. A. *Spectrochim. Acta* 1982, 38, 1307.